AD-A146 686 THE STABILITY OF AN INFINITE ELASTIC PIPE WITH UNIFORM 1/1
MEAN FLOW(U) ADMIRALTY MARINE TECHNOLOGY ESTABLISHMENT
TEDDINGTON (ENGLAND) E A SKELTON FEB 84
UNCLASSIFIED AMTE(N)/TM84057 DRIC-BR-92675 F/G 20/4 NL

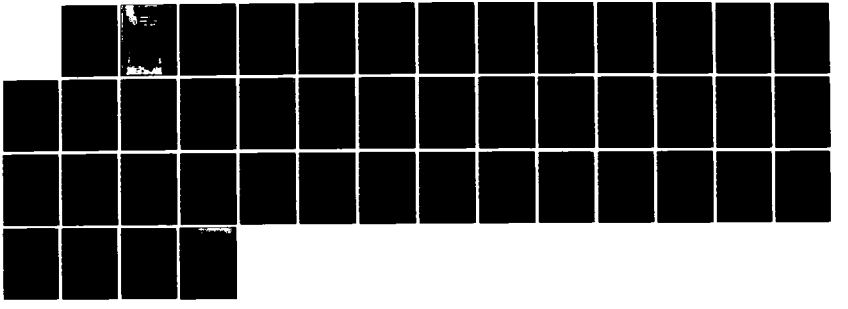

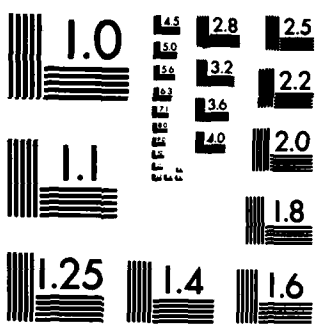

TECH MEMO AMTE (N) TM8405

COPY No 35

ADMIRALTY MARINE TECHNOLOGY ESTABLISHMENT

THE STABILITY OF AN INFINITE ELASTIC PIPE WITH UNIFORM MEAN FLOW

E. A. SKELTON

1984

UNLIMITED

AMTE(M)TM84057

THE STABILITY OF AN INFINITE ELASTIC PIPE WITH UNIFORM MEAN FLOW

BY

E A SKELTON

Summary

The pipe conveying incompressible fluid is modelled using linear beam theory. The stability of the system is analysed using a causal approach which is able to distinguish between absolute and convective instabilities. Closed-form expressions for the stability boundaries of the beam theory model are derived analytically. The dissipation-free pipe is absolutely unstable if the ratio of the mass per unit length of the pipe to that of the contained fluid is greater than one-eighth, otherwise it is convectively unstable at low excitation frequencies and stable at high frequencies. The pipe is found to be absolutely unstable when damping is included. Some numerical results are presented for a steel pipe and a rubber pipe, both of which contain water.

AMTE (Teddington)
Queen's Road
TEDDINGTON Middx TW11 0LN

42 pages
12 figures

February 1984

UNLIMITED

CONTENTS

LIST OF SYMBOLS

$W_r(z,t)$	instantaneous value of beam displacement
$F_r(z,t)$	instantaneous value of beam excitation
$W(z,t)$	displacement amplitude
$F(z,t)$	excitation amplitude
$\tilde{W}(z,\omega)$	Laplace transform of $W(z,t)$
$\bar{W}(\alpha,\omega)$	Fourier transform of $\tilde{W}(z,\omega)$
$D(\alpha,\omega)$	beam dispersion relation
t	time
α, n	axial and circumferential wavenumbers
f	frequency in Hz
ω	radian frequency ($=2\pi f$)
σ	$\mathrm{Im}[\omega]=\sigma$ denotes the line of Laplace integration
ρ_1, c_1, U_1	density, sound velocity and axial flow velocity of interior fluid
M_1	Mach number of fluid, $M_1=U_1/c_1$
a, h, ρ_s	radius, thickness and density of shell
E	Young's modulus of the shell
ν	Poisson's ratio of the shell
η	hysteretic loss factor of the shell
M	mass per unit length of fluid, $M=\pi a^2\rho_1$
m	mass per unit length of beam, $m=2\pi ah\rho_s$
I	area moment of inertia of beam, $I=\pi ha^3$
$*$	(as a superscript) denotes complex conjugate

INTRODUCTION

Much theoretical work [1-9] has been done on the vibration and sound radiation of fluid-loaded structures, such as plates and shells, excited by time-harmonic mechanical forces or acoustic point sources. These, and other, authors deal with wave propagation in, and vibration response of, systems in which the fluid is assumed to be stationary. Practical pipework systems, however, usually convey fluid whose motion may significantly change the dynamic characteristics of the system. In particular, the interchange of energy between the moving fluid and the pipe may result in an instability which causes excessive vibration and sound radiation.

The stability analysis of systems conveying fluid usually proceeds via the system dispersion relation. Complex values of frequency corresponding to real values of wavenumber are obtained and the sign of the imaginary part of these frequencies indicates whether or not the system is unstable. Dowell [10] has used this approach to investigate the flutter behaviour of infinite shells. He concludes that the shell theory used was inadequate for the n=1 harmonic, but for each n≠1 circumferential harmonic a flutter instability occurs above a critical flow speed, the lowest such speed being the one associated with the n=2 harmonic. The effect of damping in the shell was not considered.

Melcher [11] describes an alternative approach to stability analyses which was used by Briggs [12] in connection with beam-plasma interactions. This approach demands that the system is causal, that is, it cannot respond until an excitation is applied. At a sufficiently long time after the excitation has been applied three types of behaviour may be identified. Firstly, there is the stable configuration in which the response is finite everywhere in space-time. Secondly, there is the convectively unstable configuration in which the response increases exponentially with distance from the excitation. Thirdly there is the absolutely unstable configuration in which the response at all points in the system increases exponentially with time. Brazier-Smith & Scott [13] have applied this causal approach to the problem of uniform incompressible flow over an infinite undamped elastic plate. The excitation was assumed to be a time-harmonic force switched on at t=0. They found that at low excitation frequencies there are convective instabilities, and that above a critical flow velocity there are also absolute instabilities. Atkins [14] has confirmed the main results of this paper and has also demonstrated that plate damping may destabilise some free-waves at all flow speeds and does not remove the absolute instability which occurs above the critical velocity.

In the present work the causal approach to stability determination is applied to an infinite pipe with uniform axial fluid flow. The pipe is modelled as a beam conveying an incompressible fluid. The effects of pipe damping are included in the model. The stability characteristics of the beam theory model are deduced analytically, whereas a numerical approach would be necessary to determine the stability characteristics of shell theory models.

2. BEAM THEORY

The transverse displacement $W_r(z,t)$ of a pipe conveying an inviscid incompressible fluid is often assumed to satisfy the differential equation of beam theory [15], viz.,

$$EI\partial^4 W_r/\partial z^4 + MU_1^2\partial^2 W_r/\partial z^2 + 2MU_1\partial^2 W_r/\partial z\partial t + (M+m)\partial^2 W_r/\partial t^2 = F_r(z,t) \qquad (2.1)$$

where M is the mass per unit length of the fluid, m is the mass per unit length of the pipe and I is the area moment of inertia of the pipe.

The causal solution for the displacement may be obtained by expressing it as the Laplace-Fourier transform

$$W(z,t) = (1/4\pi^2)\int_{-\omega+i\sigma}^{\omega+i\sigma}\int_{-\infty}^{\infty} \frac{\bar{F}(\alpha,\omega)}{D(\alpha,\omega)} \exp(i\alpha z - i\omega t)\,d\alpha\,d\omega \qquad (2.2)$$

where the dispersion relation, $D(\alpha,\omega)$, is obtained from equation (2.1) as

$$D(\alpha,\omega) = EI\alpha^4 - MU_1^2\alpha^2 + 2MU_1\alpha\omega - (M+m)\omega^2 \qquad (2.3)$$

3. MATHEMATICAL ANALYSIS OF BEAM STABILITY

(a) General

The symmetrical nature of the dispersion relation, viz.,

$$D(\alpha,\omega) = D^*(-\alpha^*,-\omega^*) \qquad (3.1)$$

means that it is necessary to consider only those values of ω such that $Re[\omega]\geq 0$, the stability analysis with $Re[\omega]<0$ being almost identical: the root loci in the complex α-plane obtained for those ω with $Re[\omega]<0$ are reflections in the imaginary α-axis of those obtained for $Re[\omega]>0$. The analysis of beam stability is further simplified by the absence of branch cuts in the complex α-plane.

The first step in the stability analysis, as described in the Appendix, is to search for coalescing poles of the dispersion relation which originate in opposite half-planes. If such poles exist, they indicate the presence of absolute instabilities for both impulse and time-harmonic switch-on disturbances. Secondly, in the absence of coalescing poles the form of the response to the time-harmonic disturbance is determined, the response to the impulse being bounded in both space and time.

(b) Coalescing Poles

Coalescing poles are present at those values of ω_p and α_p which satisfy the simultaneous equations

$$D(\alpha,\omega)=0 \tag{3.2}$$

$$\partial D(\alpha,\omega)/\partial\alpha=0 \tag{3.3}$$

It is straightforward to solve these equations for the beam to give the two solutions

$$\omega_p=U_1^2(2M/EI)^{1/2}(1\pm\sqrt{(1-8m/M)})^{1/2}(3\pm\sqrt{(1-8m/M)})^{-3/2} \tag{3.4}$$

$$\alpha_p=U_1(M/2EI)^{1/2}(1\pm\sqrt{(1-8m/M)})^{1/2}(3\pm\sqrt{(1-8m/M)})^{-1/2} \tag{3.5}$$

where for the first solution the positive signs are taken throughout, and for the second solution the negative signs are taken throughout. The remaining two solutions of equations (3.2) and (3.3) are of opposite sign to those given above, and in particular have $Re[\omega_p]<0$. For cases where $8m/M<1$ both of the solutions for ω_p given by equation (3.4) are purely real, and therefore represent transient solutions, even if the root loci of the coalescing poles originated in opposite half-planes.

If, however, $8m/M>1$, then the second solution for (ω_p,α_p) is such that ω_p has a positive imaginary part, indicating that an absolute instability is present if the root loci of the coalescing poles originated in opposite half-planes. The corresponding value of α_p has a positive real part and a negative imaginary part. The presence of an absolute instability is determined as follows.

(i) At any real frequency ω_r, the four root loci for $\omega=\omega_r+i\sigma$, where σ is large and positive, are found from the various combinations of

$$\alpha \simeq [\sigma^2(M+m)/4EI]^{1/4}(\pm1\pm i) \tag{3.6}$$

Hence, each of the root loci originates in a separate quadrant of the complex α-plane.

(ii) In order to determine whether or not the coalescing poles originated in the same half-plane, it is convenient to solve the dispersion relation, equation (3.2), for ω, viz.,

$$\omega=\alpha[MU_1\pm\{EI(M+m)\alpha^2-mMU_1^2\}^{1/2}]/(M+m) \tag{3.7}$$

and to consider where the root loci may cross the real and imaginary α-axes.

(iii) If a root locus crosses the imaginary α-axis, at $\alpha=ir$ say, then from equation (3.7)

$$\omega=ir[MU_1\pm i\{EI(M+m)r^2+mMU_1^2\}^{1/2}]/(M+m) \tag{3.8}$$

and because, by definition, on a root locus $\mathrm{Im}[\omega]$ must be positive, equation (3.8) shows that r must also be positive. Hence, no root locus may cross the negative imaginary α-axis.

(iv) If a root locus crosses the real α-axis, at $\alpha=s$ say, then by considering the real and imaginary parts of equation (3.7)

$$(M+m)EIs^2-mMU_1^2<0 \tag{3.9}$$

and

$$\omega_r=sMU_1/(M+m) \tag{3.10}$$

Since the analysis has been restricted to only those values of ω with positive real part, equation (3.10) shows that s must also be positive. Hence, no root locus may cross the negative real α-axis. This result, together with the result of paragraph (iii) shows that the locus which originates in the lower half-plane, with $\mathrm{Re}[\alpha]<0$, must remain in that quadrant of the complex α-plane, and in particular it may not coalesce with any other loci. Thus, if the coalescing poles originate in the same half-plane, it must be the upper half-plane.

(v) Suppose that the loci of the coalescing poles both originate in the upper half-plane, then, because the imaginary part of α_p is negative, they must both cross the (positive) real α-axis. Equations (3.9) and (3.10) show that for a given real frequency ω_r, loci may cross the real α-axis at (at most) one point. By substituting this (real) value of α into equation (3.7) it is clear that only one (positive) value of σ is possible for both loci at this point. Hence, coalescence occurs on the real α-axis and a contradiction to the results of equation (3.5) has been obtained. Thus the coalescing poles may not both originate in the upper half-plane.

Together, the results of paragraphs (iv) and (v) show that the loci of the coalescing poles originate in opposite half-planes, and therefore indicate that the pipe is absolutely unstable if $8m/M>1$, and, as described in the Appendix, the pipe response is dominated by the frequency ω_p.

(c) Response to Time-harmonic Switch-on

In the absence of an absolute instability, the form of the pipe response to a forcing excitation at a particular frequency ω_0 may be determined. For $8m/M<1$ there is no absolute instability present, and the behaviour of the pipe depends on the forcing frequency. It follows from equations (3.9) and (3.10) that a locus for $\omega=\omega_0+i\sigma$ crosses the real α-axis only if

$$\omega_0<MU_1^2(M+m)^{-1}[Mm/EI(M+m)]^{1/2} \tag{3.11}$$

This is a necessary, but not sufficient, condition for a convective instability since the locus may subsequently return to the real α-axis, in which case the pole would represent a propagating wave.

By considering the dispersion relation, in the form given by equation (3.7) for real values of α and ω it is obvious that the branch

$$\omega(\alpha)=\alpha[MU_1+\{EI(M+m)\alpha^2-mMU_1^2\}^{1/2}]/(M+m) \tag{3.12}$$

is a monotonic increasing function of α, in the regions of the real α-axis where it exists as a real function. Clearly, however, the branch given by

$$\omega(\alpha)=\alpha[MU_1-\{EI(M+m)\alpha^2-mMU_1^2\}^{1/2}]/(M+m) \tag{3.13}$$

is not, and the equation

$$\omega_0=\omega(\alpha) \tag{3.14}$$

may have 2, 3, or 4 real roots α, depending on the value of ω_0. The boundaries between these intervals on the ω-axis are determined by solving the equation

$$\partial\omega/\partial\alpha=0 \tag{3.15}$$

where $\omega(\alpha)$ is given by equation (3.13). The pipe behaviour may then be descibed in each of three frequency regions, using arguments similar to those used in section 3(b). The behaviour is as follows:

For

$$\omega_0<U_1^2(2M/EI)^{1/2}(1-\sqrt{(1-\delta m/M)})^{1/2}(3-\sqrt{(1-\delta m/M)})^{-3/2} \tag{3.16}$$

the pipe is convectively unstable in the region $z>0$. In this region two waves whose phase propagates downstream from the excitation exist, one of which decays exponentially with distance, whilst the other grows exponentially with distance. In the upstream region, $z<0$, there are two free-waves which propagate without decay, one whose phase propagates downstream and the other upstream. However, the group velocity, $\partial\omega/\partial\alpha$, of both of these waves is negative, indicating that in both cases the energy flows upstream from the source of excitation.

For $\omega_0>U_1^2(2M/EI)^{1/2}(1-\sqrt{(1-\delta m/M)})^{1/2}(3-\sqrt{(1-\delta m/M)})^{-3/2}$

and $\omega_0<U_1^2(2M/EI)^{1/2}(1+\sqrt{(1-\delta m/M)})^{1/2}(3+\sqrt{(1-\delta m/M)})^{-3/2}$ (3.17)

the pipe behaviour is stable and consists of four free-waves. In the upstream region, $z<0$, the phase of one wave propagates upstream from the point of excitation, whilst the phase of the other propagates downstream from infinity. Again, in both cases, the group velocity is negative and the energy flow is upstream from the point of excitation. In the region, $z>0$, the phase of both free-waves propagates downstream from the source. The group velocity of both of these waves is positive, and the energy flow of each wave is downstream from the source of excitation unless

$$\omega_0< MU_1^2(M+m)^{-1}[Mm/EI(M+m)]^{1/2}$$

when the group velocity of one of the waves is negative, and the energy flow associated with that wave is upstream from infinity.

For

$$\omega_0 > U_1^2 (2M/EI)^{1/2} (1+\sqrt{(1-8m/M)})^{1/2} (3+\sqrt{(1-8m/M)})^{-3/2} \qquad (3.18)$$

the pipe behaviour is stable and consists only of propagating and decaying waves. In the downstream region, $z>0$, two waves travel downstream from the source, one of which is a free-wave which propagates without decaying and the other is evanescent and decays exponentially with distance. In the upstream region, $z<0$, one free-wave propagates upstream without decaying. The amplitude of the second wave in the $z<0$ region decays exponentially with distance from the excitation and is therefore stable.

(d) Effect of Damping

A positive hysteretic loss factor, η, may be introduced into the mathematical model by making E complex, viz.,

$$\begin{aligned} E &= E(1-i\eta), \quad \text{for } \omega>0 \\ E &= E(1+i\eta), \quad \text{for } \omega<0 \end{aligned} \qquad (3.19)$$

where η is small compared with unity. The symmetry of the dispersion relation, equation (3.1), is preserved which means that it is again sufficient to consider only those values of ω with $Re[\omega]>0$.

Equations (3.4) and (3.5) again give the position of coalescing poles except that now, for small η,

$$\begin{aligned} \omega_p &= \omega_p (1+i\eta/2) \\ \alpha_p &= \alpha_p (1+i\eta/2) \end{aligned} \qquad (3.20)$$

For the case $8m/M>1$, the addition of damping has altered the location of the coalescing poles slightly, but not enough to stabilise the system from its previously absolutely unstable state.

For the case $8m/M<1$, where there was no absolute instability, the addition of damping alters the position of the root loci slightly, and may result in coalescing poles. In the absence of damping, both solutions for the frequency, given by equation (3.4), at which poles coalesce were real and thus represented transient solutions. Equation (3.20) shows that with damping both of these solutions have a positive imaginary part, and may therefore represent absolute instabilities if the coalescing poles originated in opposite half-spaces. The behaviour of the root loci in the undamped case show that at the lower frequency the coalescence is between loci which both originate in the upper half of the complex α-plane, but at the higher frequency

$$\omega_p = U_1 (2M/EI)^{1/2} (1+\sqrt{(1-8m/M)})^{1/2} (3+\sqrt{(1-8m/M)})^{-3/2} \qquad (3.21)$$

the coalescence is between one pole whose locus originates in the lower half-space and one whose locus originates in the upper half-space. There is thus an absolute instability at the frequency ω_p given by equation (3.21). However, because the exponential growth rate is proportional to η, which is small, this contribution to the displacement may not dominate the solution until t becomes very large. For small or moderate values of the time t, the response will appear to be approximately as was determined for the undamped case.

4. NUMERICAL RESULTS

(a) General

Fortran programs have been written for calculating the complex roots, α, of the dispersion relation given by equation (2.3) for complex values of the frequency parameter $\omega=\omega_r+i\sigma$. The programs are written in double precision complex arithmetic, which is simulated [16] by the use of double precision real arrays of leading dimension two. This was necessary because the programs were run on a PDP-11 computer whose single precision arithmetic word length of 32 bits is inadequate for this type of problem.

The material and geometric constants, in SI units, which were used in the calculations for Figures 6-11 are as follows:

Steel Pipe: $E=19.5\times10^{10}$ $\nu=0.29$ $\rho=7700.0$ $a=1.0\times10^{-2}$ $h=0.05\times10^{-2}$

Rubber Pipe: $E=0.23\times10^{10}$ $\nu=0.4$ $\rho=1100.0$ $a=1.0\times10^{-2}$ $h=0.05\times10^{-2}$

Water: $\rho=1000.0$ $c=1500.0$ $U=10.0$

Damping in the pipe wall was included in the calculations for Figures 10 and 11 by setting E, the Young's modulus, to the complex value $E(1-i\eta)$, where the numerical value of η, the hysteretic loss factor, was chosen as 0.2. This value, which is an order of magnitude higher than practical levels, helps to clarify the effect of damping without significant change to the physical interpretation.

(b) Beam Theory Results

Figures 6a and 6b show the real and imaginary parts, respectively, of the wavenumber-frequency plot for the undamped steel pipe, obtained from the dispersion relation for a beam, equation (2.3). The branches labelled 1 and 2 are purely real, and branches 3 and 4 are complex conjugate roots.

The positive real branch, labelled 1, has a minimum value at approximately 0.19Hz which indicates an infinite group velocity and also a possible instability at this frequency. Clearly, because these branches of the dispersion relation do not intersect, no poles may coalesce at real values of the frequency.

Figure 7 shows a root locus stability plot for the four roots (labelled a, b, c and d) of the undamped steel pipe. All the loci labelled 1 correspond to the frequency $\omega_r/2\pi$=0.04Hz. The loci labelled 1a and 1b terminate on the real α-axis and for a time-harmonic switch-on excitation at this frequency therefore represent free-waves, whose phase propagates upstream from the excitation and downstream from infinity, respectively. The energy of both of these waves propagates upstream from the excitation. The locus labelled 1c crosses the real α-axis and terminates in the lower half-plane. This represents a convectively unstable wave propagating downstream from the excitation. The locus labelled 1d terminates in the upper half-plane, and, because there are no branch cuts in the complex α-plane, may be identified with an evanescent wave propagating downstream from the excitation.

The loci labelled 2 and 3 correspond to frequencies $\omega_r/2\pi$=0.08Hz and $\omega_r/2\pi$=0.12Hz, respectively, and represent responses similar to those at 0.04Hz. The loci labelled 4 and 5, corresponding to frequencies $\omega_r/2\pi$=0.16Hz and $\omega_r/2\pi$=0.20Hz, however show very different behaviour. The locus labelled 4b terminates in the lower half-plane, and may be identified with a wave whose phase and group velocities both propagate downstream from infinity. The amplitude of this wave decays exponentially with distance from the excitation point, z=0, and, according to Melcher's classification it must therefore be described as stable. In fact the amplitude of this wave increases in the direction of propagation, i.e. it appears to be a convectively unstable wave propagating downstream from infinity. The locus labelled 4c terminates on the real α-axis and represents a free-wave whose phase propagates downstream from the excitation, but whose group velocity is negative. The loci 4b and 4c therefore both represent waves whose energy propagates towards the excitation point. The locus labelled 5c terminates on the real α-axis and represents a free-wave which propagates downstream from the excitation.

The difference in the character of the response at frequencies below 0.12Hz and that at frequencies above 0.16Hz, together with the form of the response at 0.16Hz, suggests that at some frequency between these values there may be a branch point in the complex ω-plane, as a result of poles from opposite half-spaces of the complex α-plane coalescing. The form of the root loci shown in Figure 7, show that such a pair of coalescing poles must exist, and hence that the pipe has an absolute instability which exists for both the impulse excitation and the time-harmonic switch-on excitation whatever the value of ω_0, the excitation frequency. Further numerical work, not presented here, reveals that the coalescing poles are located at

$$\alpha_p = 0.18-0.05i \qquad (4.1)$$

$$\omega_p/2\pi = 0.14+0.06i \qquad (4.2)$$

which may also be obtained directly from equations (3.4) and (3.5). The component of the pipe response due to the integral around the branch cut in the complex ω-plane grows exponentially with time, and at large times the response is approximately at the frequency ω_p and wavenumber α_p, given by

equations (4.1) and (4.2). The frequency at which the absolute instability occurs, equation (4.2), does not coincide with the frequency, obtained from Figure 6, at which the group velocity appears to be infinite.

Figures 8a and 8b show the real and imaginary parts, respectively, of the wavenumber-frequency plot for the undamped rubber pipe, obtained from the dispersion relation for a beam, equation (2.3). The branches labelled 1 and 2 are purely real, and branches 3 and 4 are complex conjugate roots. At frequencies between f_L (approximately 1.2Hz) and f_U (approximately 1.3Hz), the number of real positive roots of the dispersion relation changes from one to three. At frequencies below f_L a pair of complex conjugate roots exist, which coalesce at $f=f_L$. At frequencies between f_L and f_U all four roots are real. At f_U the two largest real roots coalesce, and at higher frequencies this pair of roots are complex conjugates.

Figure 9 shows a root locus stability plot for the four roots (labelled a, b, c and d) of the undamped rubber pipe. All the loci labelled 1 correspond to the frequency $\omega_r/2\pi=0.75$Hz. The loci labelled 1a and 1b terminate on the real α-axis and represent free-waves whose phase propagates upstream from the excitation and downstream from infinity, respectively. The energy of both of these waves propagates upstream from the excitation. The locus labelled 1c crosses the real α-axis and terminates in the lower half-plane, whilst the locus labelled 1d terminates in the upper half-plane. These represent a convectively unstable wave and an evanescent wave, resectively, both propagating downstream from the excitation. The loci labelled 2 correspond to the frequency $\omega_r/2\pi=1.0$Hz, and are similar to those at 0.75Hz.

The loci labelled 3 in Figure 9 correspond to the frequency $\omega_r/2\pi=1.25$Hz. The loci labelled 3a and 3b terminate on the real α-axis and represent free-waves propagating upstream from the excitation. The loci labelled 3c and 3d also both terminate on the real α-axis and represent free-waves whose phase propagates downstream from the excitation, but whose energy propagates upstream from infinity and downstream from the excitation, respectively.

The loci labelled 4 correspond to the frequency $\omega_r/2\pi=1.5$Hz. The locus labelled 4a terminates on the real α-axis and therefore represents a free-wave propagating upstream from the excitation. The locus labelled 4b terminates in the lower half-plane, and represents a wave whose amplitude decays exponentially with distance from the excitation point. The locus labelled 4c terminates on the real α-axis and represents a free-wave propagating downstream from the excitation, whilst the locus labelled 4d terminates in the upper half-plane and represents a wave whose amplitude decays exponentially with distance from the excitation point. The waves represented by the loci 4b and 4d have positive phase speeds, but zero group velocities. The loci labelled 5 correspond to the frequency $\omega_r/2\pi=1.75$Hz, and are similar to those at 1.5Hz.

The only coalescing poles which originate in opposite half-planes coalesce at a real frequency between 1.25Hz and 1.5Hz. It is shown in the Appendix that coalescence at a real frequency corresponds to a transient response, and the rubber pipe therefore has no absolute instability. The pipe response is predominantly at the excitation frequency, and the nature of the response depends on the value of the excitation frequency. If the excitation frequency is less than f_L the pipe is convectively unstable. If the excitation frequency is between f_L and f_U the reponse consists only of

free-waves, and if the excitation frequency is greater than f_U the response is again stable and consists only of free-waves, an evanescent wave propagating downstream from the excitation and a wave whose phase propagates downstream from infinity, but whose amplitude decays exponentially with distance from the excitation. The values of f_L and f_U may be obtained either by further numerical work, or directly from equations (3.16) and (3.18). For the rubber pipe they are found to be

$$f_L = 1.24\text{Hz} \tag{4.3}$$

$$f_U = 1.26\text{Hz} \tag{4.4}$$

The numerical results presented in Figures 7 and 9 were repeated with pipe damping included in the calculations. The numerical value of η, the hysteretic loss factor, was chosen to be 0.2, and the results are shown in Figures 10 and 11. The positions of the root loci for the steel pipe, shown in Figure 10, are only slightly altered by the addition of damping. In particular, the loci corresponding to free-waves propagating upstream with negative phase speed in the undamped case, move downwards, i.e. away from the axis, and therefore represent evanescent waves propagating upstream. The loci corresponding to free-waves propagating upstream from the excitation with positive phase speed in the undamped case, move upwards, i.e. they cross the real α-axis, and therefore represent unstable waves whose amplitudes increase with distance from the excitation. However, it is clear from Figure 10 that a locus from the upper half-plane must coalesce with a locus from the lower half-plane at a complex frequency whose real part is between 0.12Hz and 0.16Hz and that the pipe is therefore absolutely unstable. Whilst the addition of damping to the pipe may stabilise or destabilise individual free-waves which propagate at the excitation frequency, it does not remove the absolute instability, which dominates the solution at large times.

The positions of the root loci for the rubber pipe, shown in Figure 11, are again only slightly altered by the addition of damping. The individual free-waves propagating at the excitation frequency may be stabilised or destabilised in the same way as for the steel pipe. However, at a frequency of approximately 1.25Hz a root locus from the upper half-plane coalesces with one from the lower half-plane at a complex value of ω_p, indicating an absolute instability. Whilst the addition of damping to the pipe may stabilise or destabilise the individual free-waves at the excitation frequency its net effect is to destabilise the pipe by introducing an absolute instability which dominates the solution at large times irrespective of the excitation frequency. Thus the convective instability at low excitation frequencies is converted to the more serious absolute instability which occurs not only for all excitation frequencies but also for impulse excitations.

The stability characteristics of an undamped pipe, obtained from the beam theory model, are summarised in Figure 12. If $\delta m/M>1$ the pipe response is absolutely unstable for both the impulse excitation and the time-harmonic switch-on. If $\delta m/M<1$ the response to the impulse excitation is stable, being bounded in both space and time. The response to the time-harmonic switch-on may be convectively unstable or stable, consisting only of free-waves or of a combination of free-waves and evanescent waves, depending on the parameters of the pipe, the fluid and the excitation frequency.

5. CONCLUDING REMARKS

The stability characteristics of a pipe conveying inviscid fluid have been examined using a causal approach which is able to distinguish between an absolute instability, in which the amplitude of the response grows with time everywhere, and a convective instabilty, in which the amplitude of the response grows as the disturbance propagates away from the excitation. Two types of initial disturbance were considered; type A, which is an impulse applied at t=0, and type B, which is a time-harmonic disturbance, $\sin(\omega_0 t)$, which is switched on at t=0. If an absolute instability is present the oscillatory part of the response is dominated by the 'pinch' frequency, ω_p, whilst if a convective instability only is present the oscillatory part of the response is predominantly at the excitation frequency, ω_0.

The main findings of the mathematical and numerical work on the beam theory model were:

(i) If $\beta m/M>1$, the undamped beam has an absolute instabilty for both type A and type B disturbances. One mode of the response grows exponentially with time everywhere, and eventually dominates the variety of other wave motions which may also be present.

(ii) If $\beta m/M<1$, the undamped beam response to type A disturbances is transient everywhere. For type B disturbances the form of the response depends on the excitation frequency as follows:

(a) At excitation frequencies, ω_0, less than a small value, ω_L, the beam is convectively unstable. Its response consists of two free-waves, the direction of whose group velocities are upstream from the excitation, together with an evanescent wave and a convectively unstable wave whose group velocities are downstream from the excitation.

(b) At excitation frequencies, ω_0, in a range ω_L to ω_U, the beam is stable. Its response consists of four free-waves, two of whose group velocities are upstream from the excitation and the other two of which are downstream from the excitation.

(c) At excitation frequencies, ω_0, greater than ω_U, the beam is also stable, its response consisting of an evanescent wave and a free-wave whose group velocity is upstream from the excitation, and an evanescent wave and a free-wave whose group velocity is downstream from the excitation.

(iii) The addition of damping cannot remove an absolute instability, and it introduces one for both type A and type B excitations if one is not already present, the exponential growth factor in this case being proportional to the loss-factor, η. Because the loss-factor is usually small, it is expected that the medium term behaviour of the beam will be as described in (i) or (ii) above, but the long term behaviour must be absolutely unstable.

Some numerical work, not presented here, has also been done [17] on the stability of a pipe which is modelled using a shell theory. The main findings of this work were:

(i) For the n=0 harmonic, the shell's axisymmetric mode, two notable features emerge, viz.:

(a) Instabilities were not present for the geometric and material constants of the pipes considered in Section 4.

(b) Because the n=0 shell mode must limit to the line-excited plate problem [14] as the shell radius tends to infinity, some additional numerical and analytical work was done which suggested that convective instabilities occur only if

$$a/h > E(M_1^{-2} - 1)/2\rho_1 c_1^2 \qquad (5.1)$$

This identity is unlikely to be satisfied for most practical pipework systems which convey water.

(ii) For the n=1 harmonic, the shell's 'beam' mode, the results were identical to those of the beam theory model, as described above, at the low frequencies at which instabilities occur.

(iii) For the n=2 harmonic, the first of the shell's 'lobar' modes, two points are worthy of note, viz.:

(a) Again instabilities were not present for the geometric and material constants of the pipes considered in Section 4.

(b) Further numerical work suggested, tentatively, that convective instabilities (and hence also the possibility of absolute instabilities) may be found if the pipe radius is increased sufficiently. No formulae were obtained for this, but it is thought that the identity would be less strict than equation (5.1).

An interesting side-effect of the fluid flow is the generation of modes whose phase and group velocities are in opposite directions. However, one must be very careful in interpreting the group velocity as the velocity of energy flow when instabilities are present because some modes admit of an infinite group velocity, which is clearly not a physical possibility.

Whilst the theory presented here may be applied to the determination of approximate stability boundaries, its practical usefulness may be limited by several factors. First, the approximations which are implicit in the governing equation of motion do not adequately describe all possible flow configurations, some of which may result in other forms of instability. For example, thin, possibly turbulent boundary layers which may exist next to the pipe surface are not included in this theory. The model is, however, believed to contain the essential features of low-frequency transverse vibration. Secondly, the linear theory used here should predict the occurrence of instabilities, but, once an instability exists its amplitude and hence its practical import-

ance will be determined by non-linear effects. Thirdly, the results presented here are for infinite pipes, and the finite length of practical piping systems may not admit the long wavelength instabilities predicted. Finally, the destabilising effect of damping may render meaningless the analysis of the undamped case because some damping is always present in practice. The best way to test the range of applicability of the theory is to conduct experimental tests.

E. A. Skelton (HSO)

Manuscript completed January 1984.

REFERENCES

1. JUNGER, M.C., FEIT, D., Sound Structures and their Interaction, MIT Press (1972).

2. FEIT, D., Pressure radiated by a point-excited elastic plate, J. Acoust. Soc. Am. 40(6) pp1489-1494 (1966).

3. CRIGHTON, D.G., The free and forced waves on a fluid-loaded elastic plate, J. Sound Vibr. 63(2) pp225-235 (1979).

4. SPICER, W.J., Acoustic intensity vectors from an infinite plate with line attachments, Admiralty Marine Technology Establishment, Teddington, AMTE(N)TM81086, October 1981.

5. FULLER, C.R., FAHY, F.J., Characteristics of wave propagation and energy distribution in cylindrical elastic shells filled with fluid, J. Sound Vibr. 81(4) pp501-508 (1982).

6. FULLER, C.R., The input mobility of an infinite circular cylindrical elastic shell filled with fluid, J. Sound Vibr. 87(3) pp409-427 (1983).

7. JAMES, J.H., Sound radiation from fluid filled pipes, Admiralty Marine Technology Establishment, Teddington, AMTE(N)TM81048, September 1981.

8. JAMES, J.H., Computation of acoustic power, vibration response and acoustic pressures of fluid-filled pipes, Admiralty Marine Technology Establishment, Teddington, AMTE(N)TM82036, May 1982.

9. SKELTON, E.A., Sound radiation from a cylindrical pipe composed of concentric layers of fluids and elastic solids, Admiralty Marine Technology Establishment, Teddington, AMTE(N)TM83007, January 1983.

10. DONELL, E.H., Flutter of infinitely long plates and shells. Part 11: Cylindrical shell. AIAA J. 4(9) pp1510-1518 (1966).

11. MELCHER, J., Continuum Electromechanics, MIT Press (1981).

12. BRIGGS, R.J., Electron-stream Interaction with Plasmas, Monograph No. 29 MIT Press (1964).

13. BRAZIER-SMITH, P.R., SCOTT, J.F., The influence of flow on flexural waves, Proc. Inst. Acoustics Conf. on Advances in Underwater Acoustics, AUWE Portland (1981).

14. ATKINS, D.J., The effect of uniform flow on the dynamics and acoustics of force-excited infinite plates, Admiralty Marine Technology Establishment, Teddington, AMTE(N)TM82087, December 1982.

15. BLEVINS, R.D., Flow Induced Vibration, Van Nostrand Reinhold (1977).

16. SPICER, W.J., Free-wave propagation in and sound radiation by layered media with flow, Admiralty Marine Technology Establishment, Teddington, AMTE(N)TM82102, December 1982.

17. SKELTON, E.A., Unpublished work, 1984.

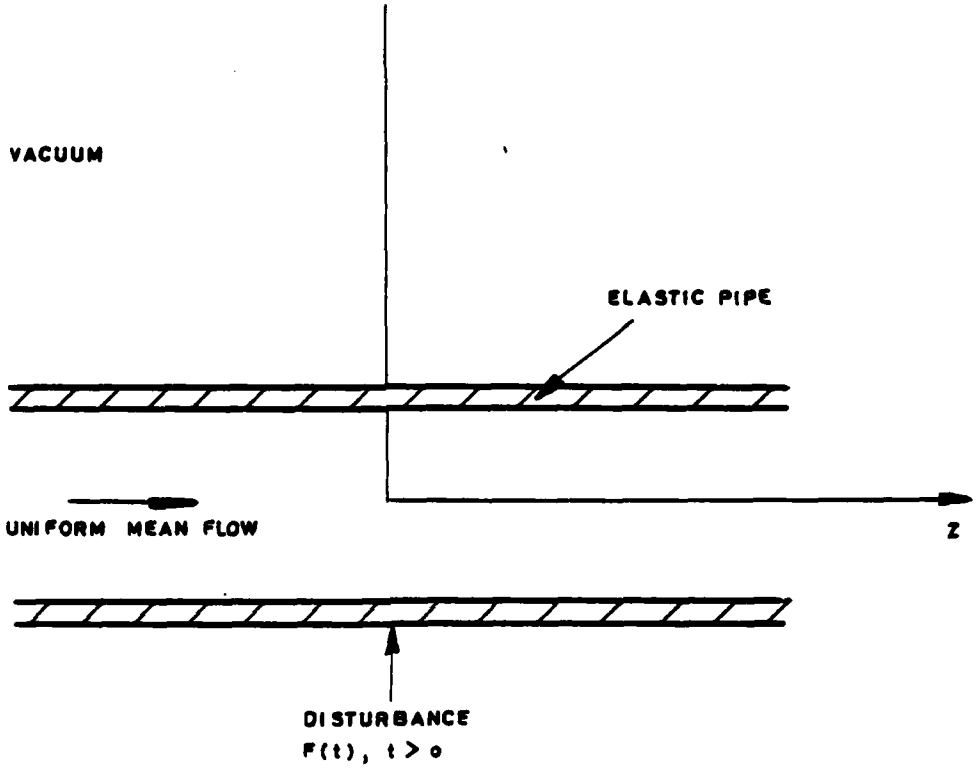

FIG. 1 PIPE WITH UNIFORM MEAN FLOW

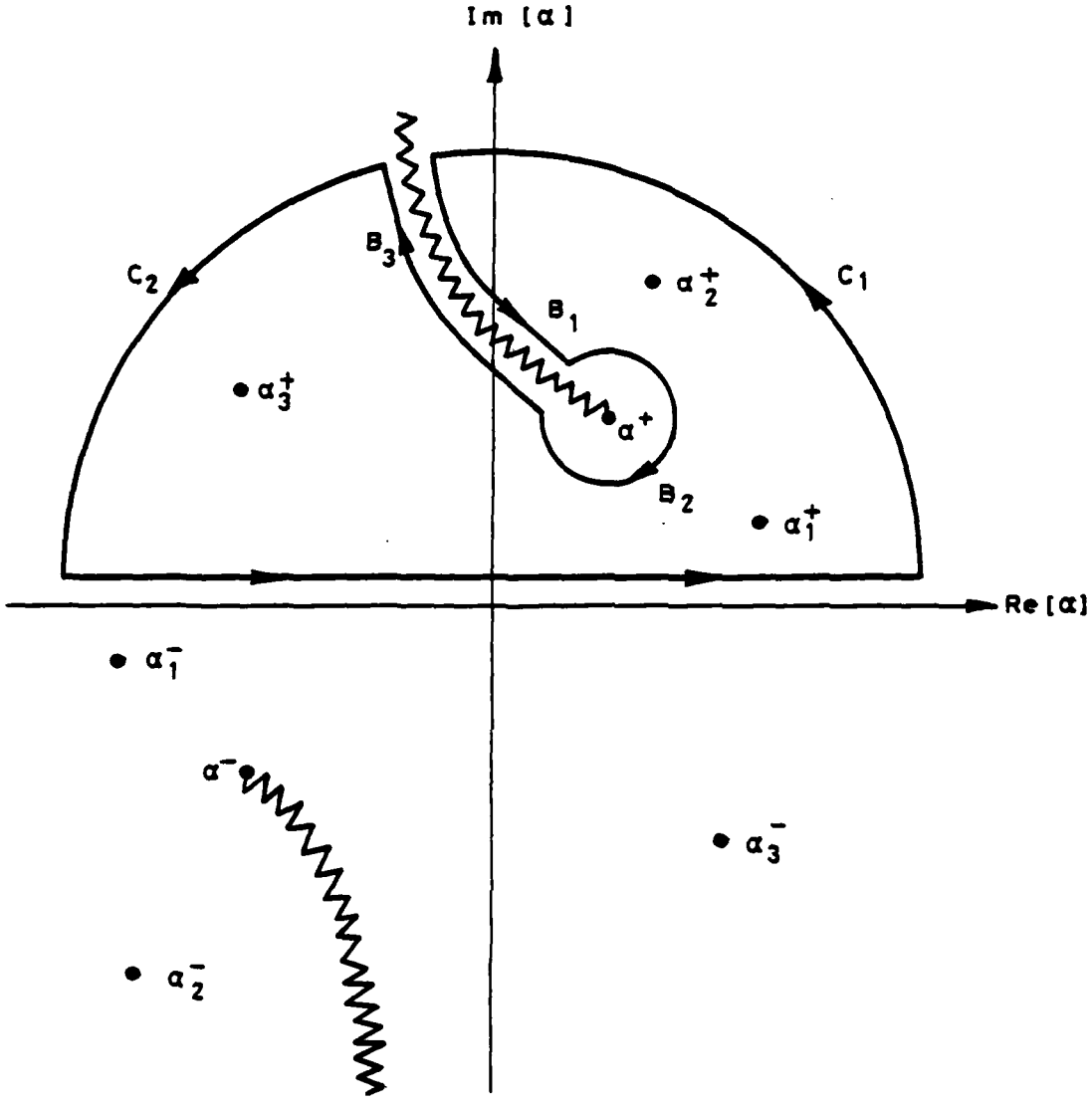

FIG. 2 CLOSURE OF THE FOURIER CONTOUR

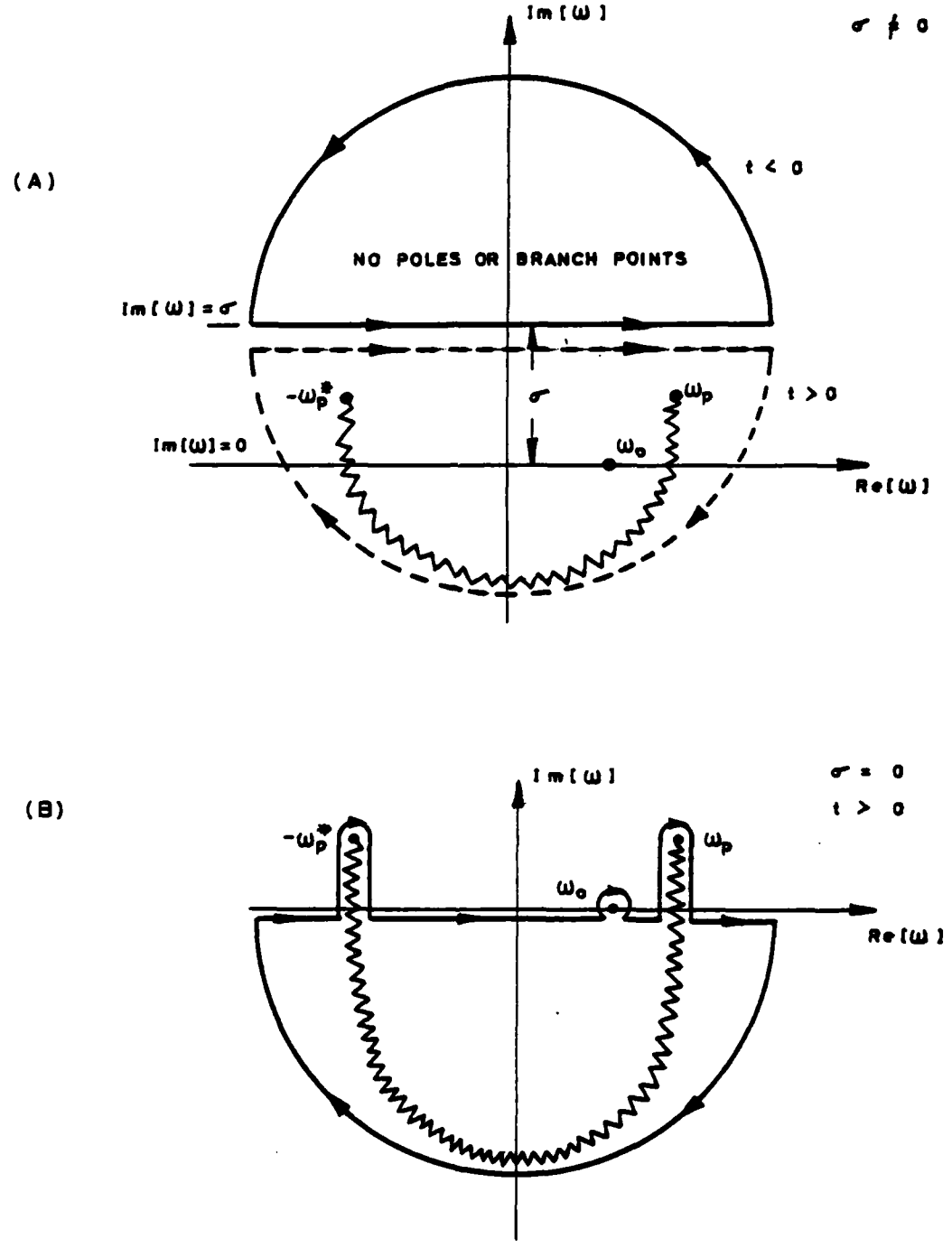

FIG. 3 CLOSURE OF THE LAPLACE CONTOUR

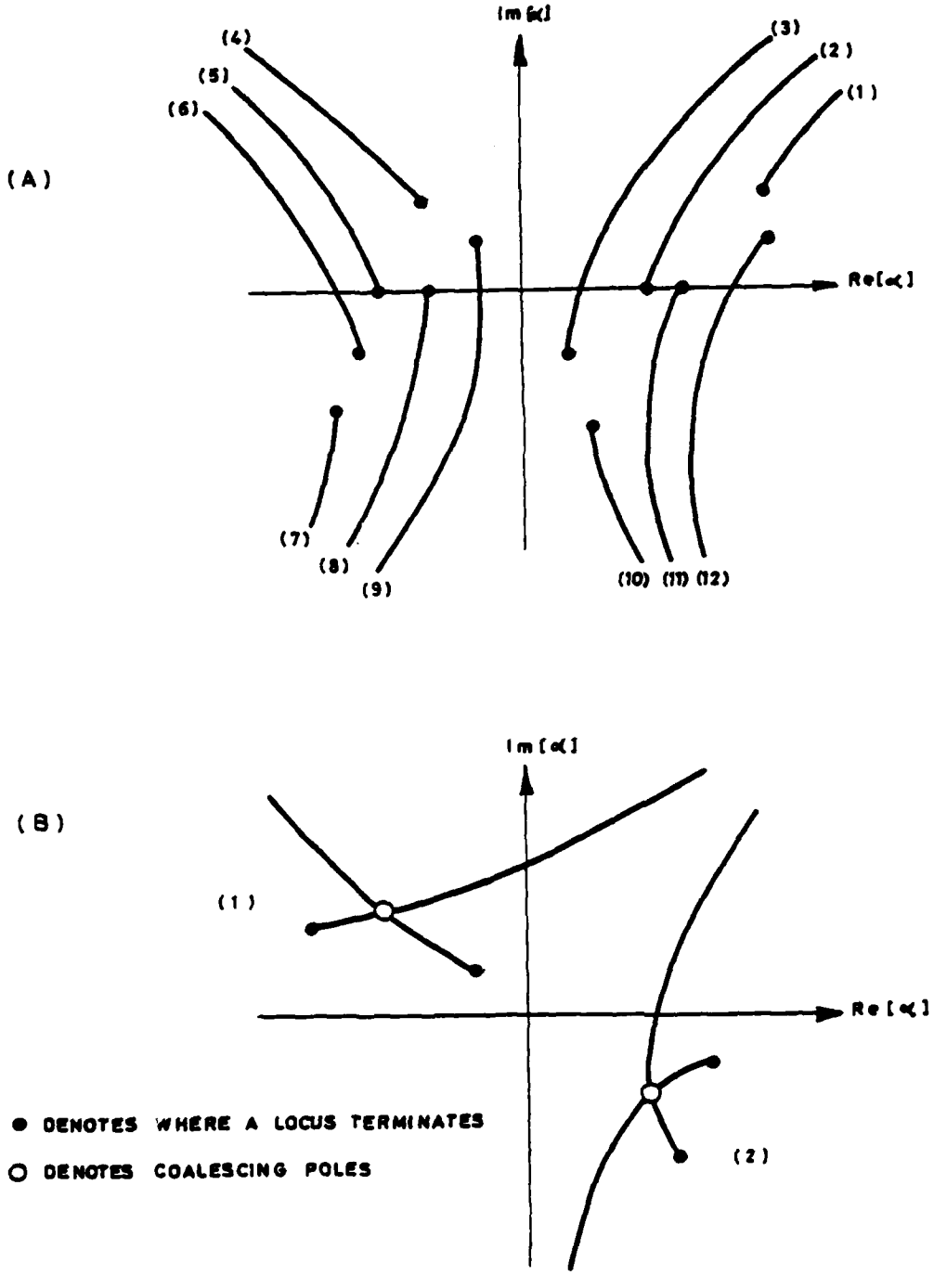

FIG. 4 EXAMPLES OF ROOT LOCI AND COALESCING POLES

(A)

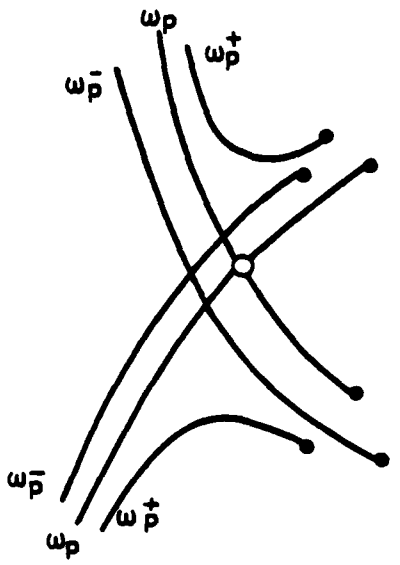

(B)

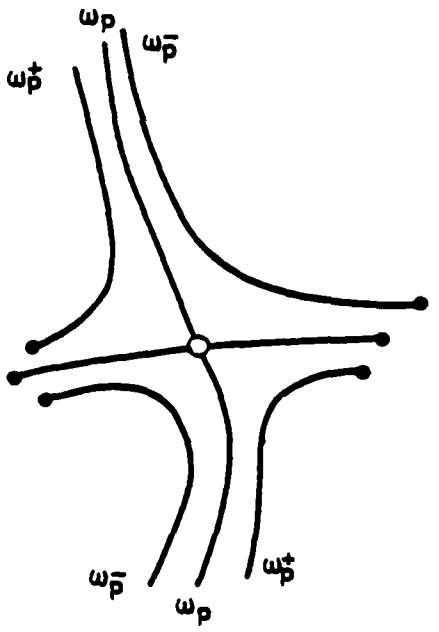

FIG. 5 EXAMPLES OF ROOT LOCI NEAR COALESCING POLES

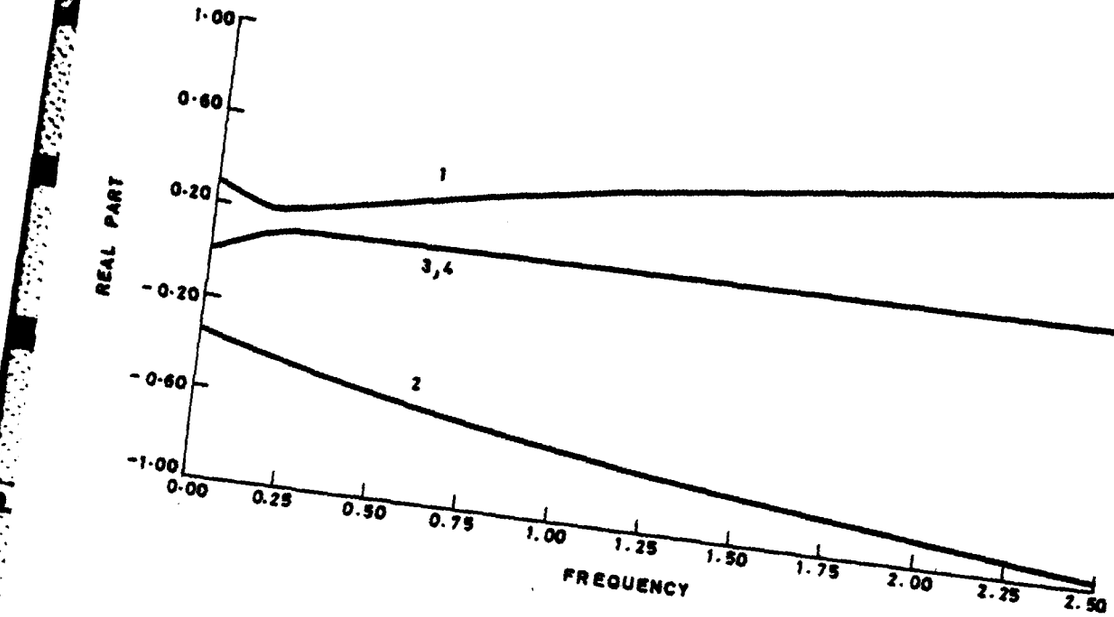

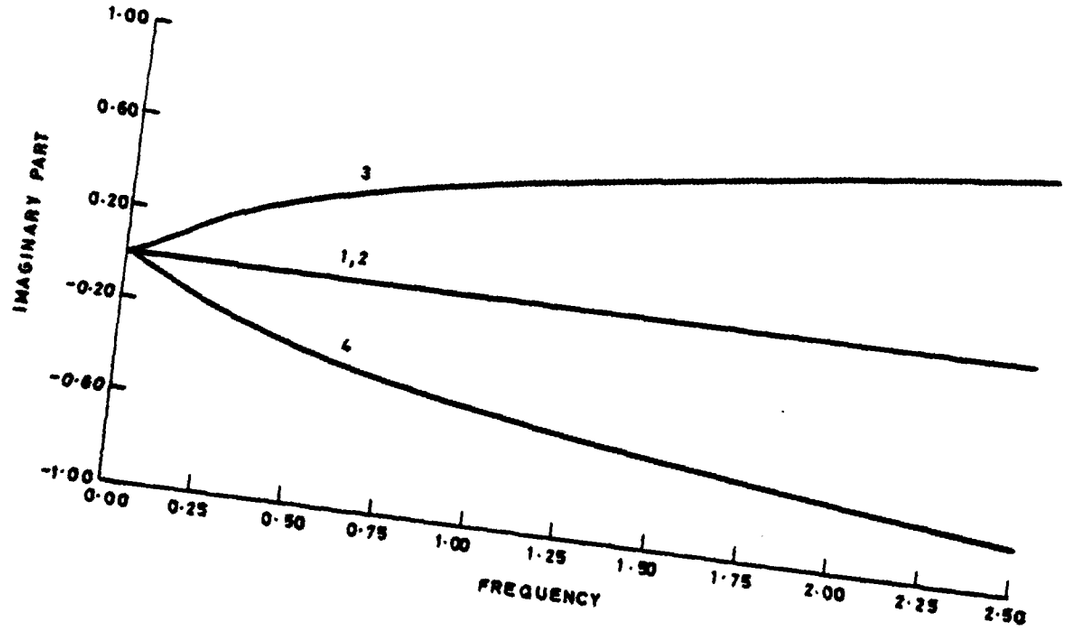

FIG. 6 WAVENUMBER VERSUS FREQUENCY PLOTS STEEL PIPE

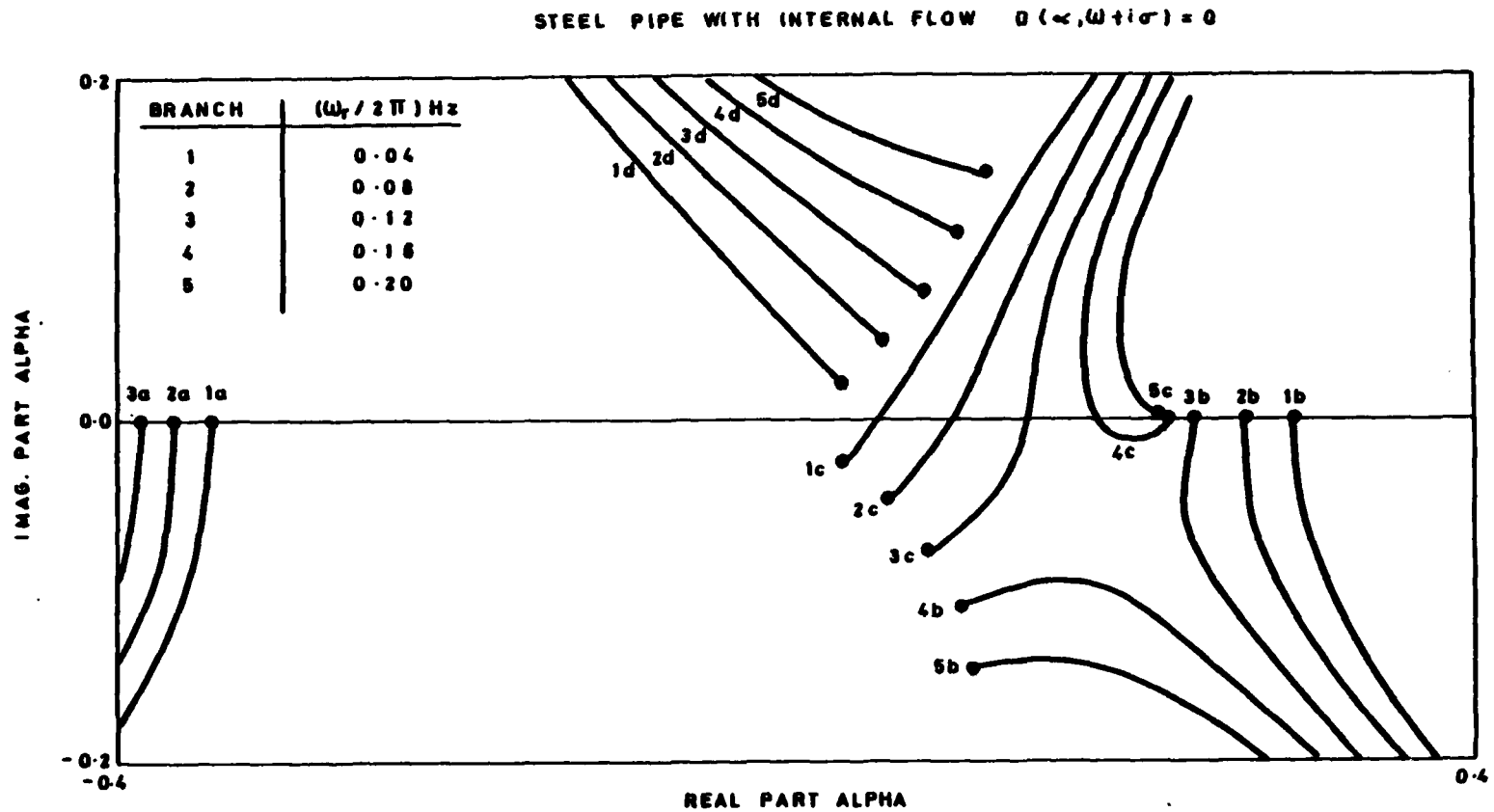

FIG. 7 THE FOUR (a, b, c, d) ROOT LOCI OBTAINED BY VARYING σ FROM LARGE POSITIVE TO ZERO BEAM THEORY U = 10 M/S ETA = 0·0

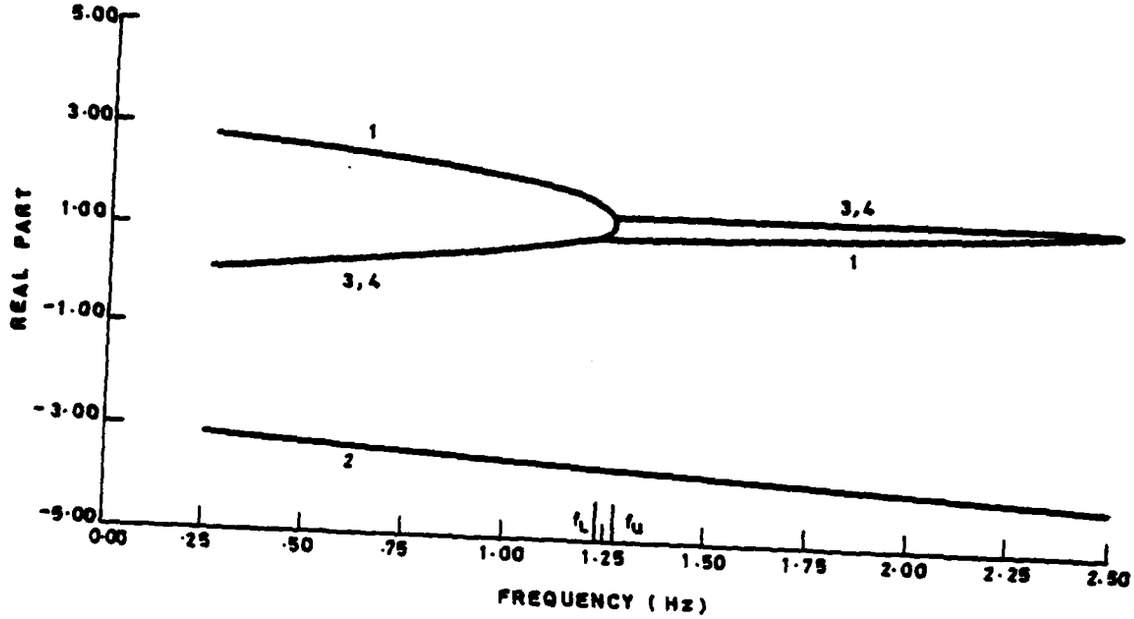

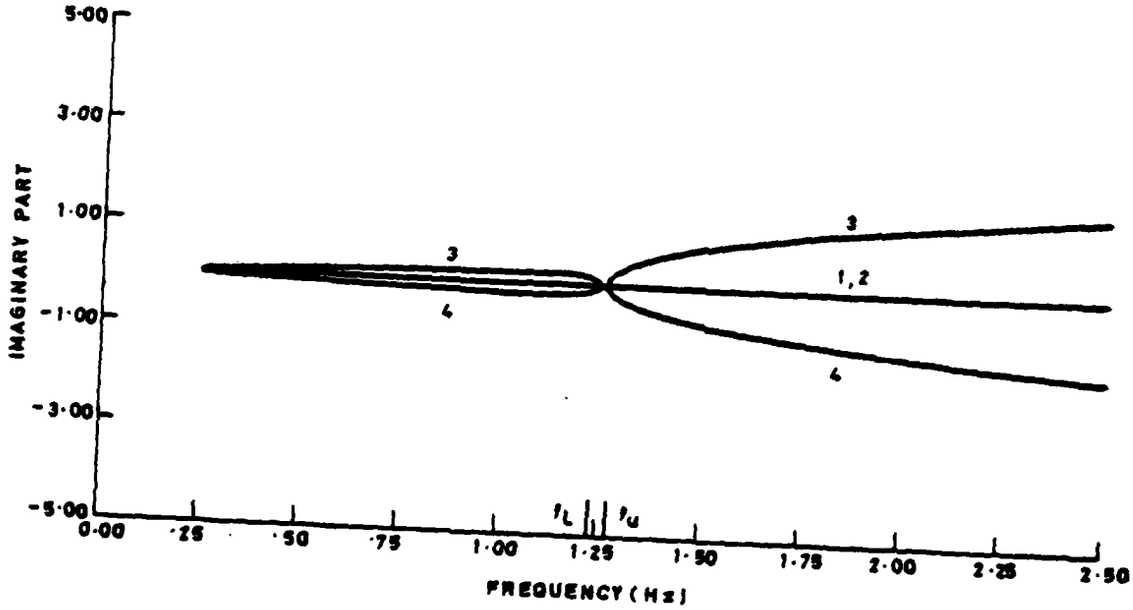

FIG. 8 WAVENUMBER VERSUS FREQUENCY PLOTS RUBBER PIPE

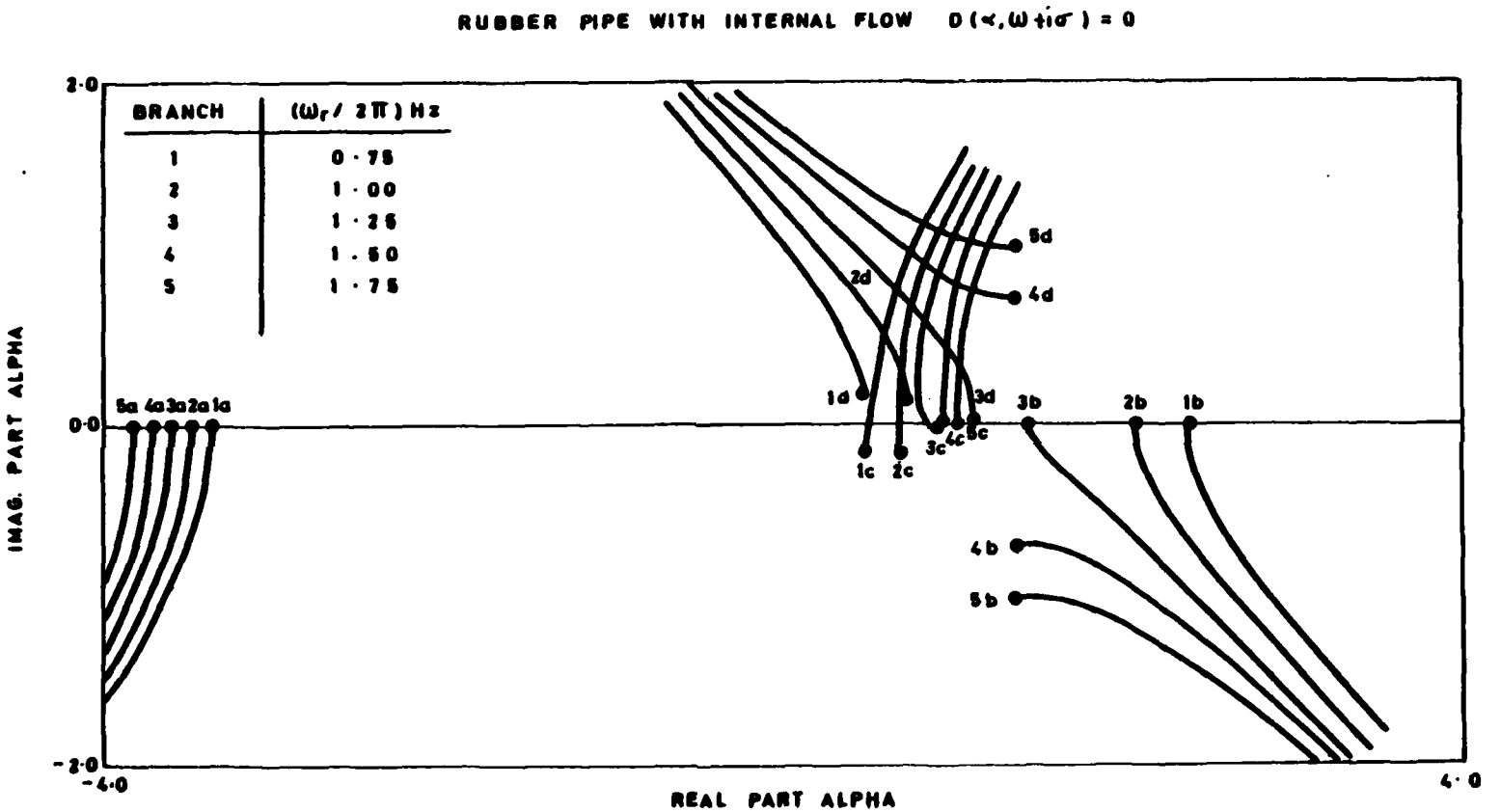

FIG. 9 THE FOUR (a,b,c,d) ROOT LOCI OBTAINED BY VARYING σ FROM LARGE POSITIVE TO ZERO BEAM THEORY U = 10 M/S ETA = 0·0

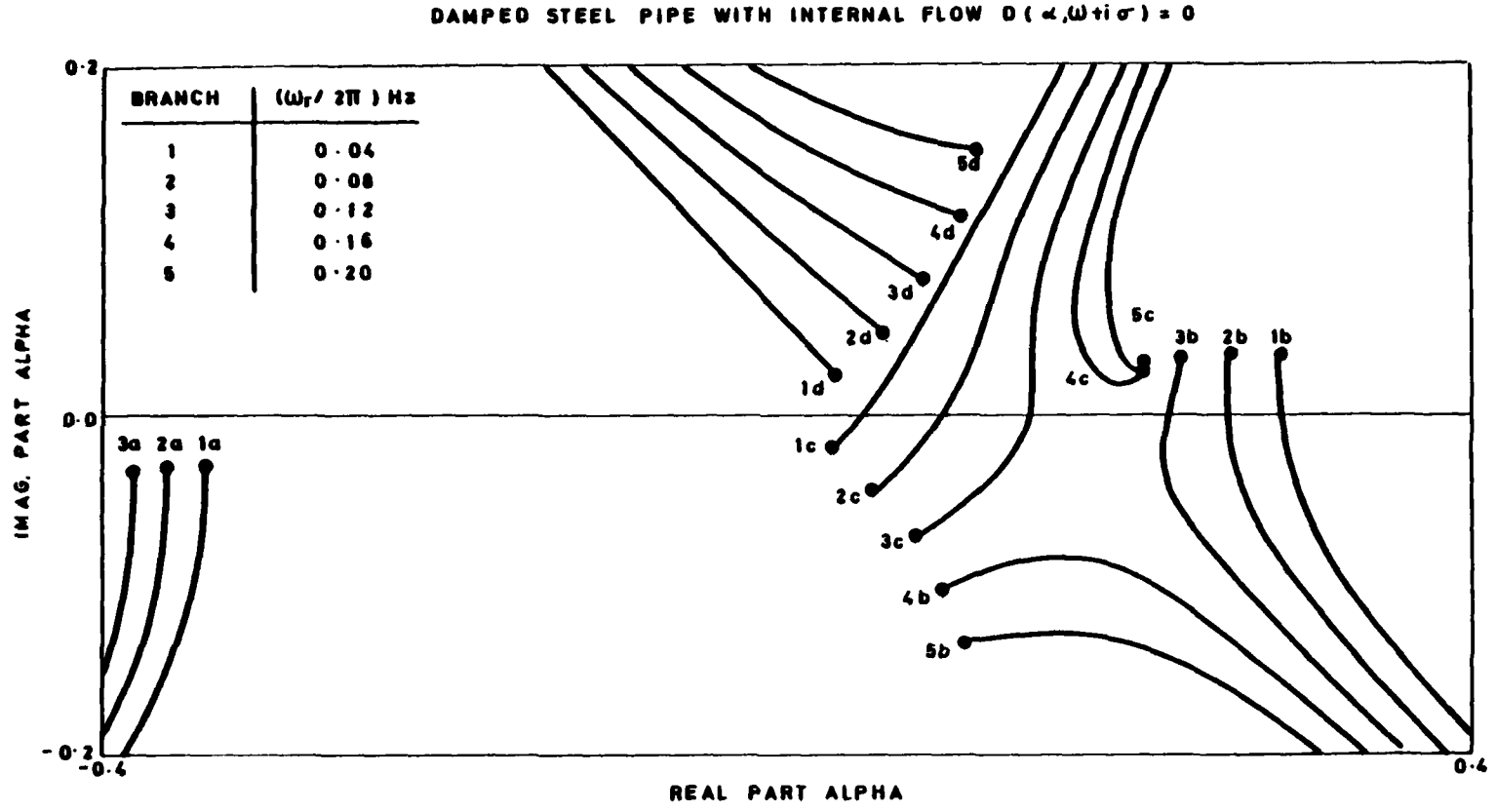

FIG. 10 THE FOUR (a, b, c, d) ROOT LOCI OBTAINED BY VARYING σ FROM LARGE POSITIVE TO ZERO BEAM THEORY U = 10 M/S ETA = 0·2

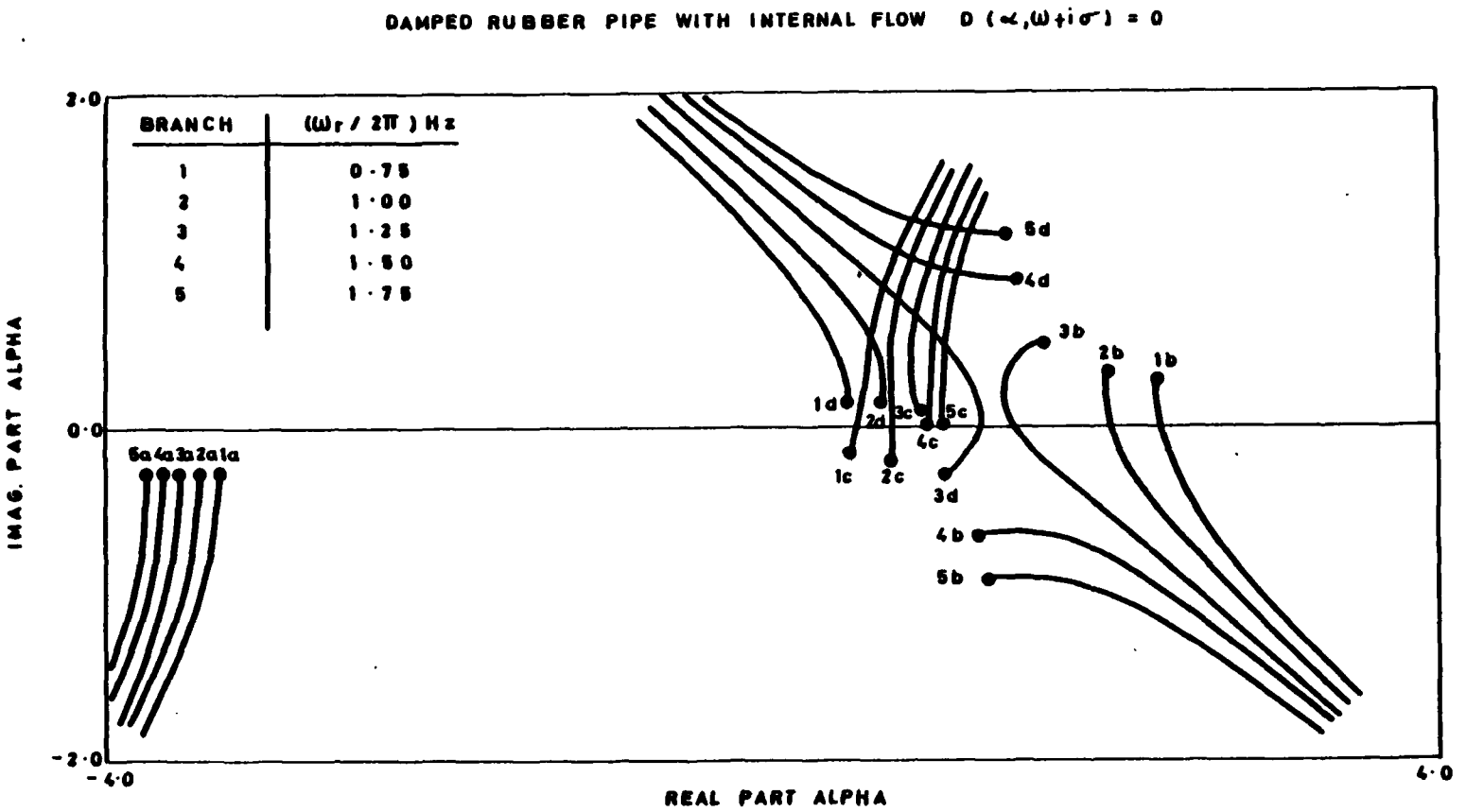

FIG. 11 THE FOUR (a, b, c, d) ROOT LOCI OBTAINED BY VARYING σ FROM LARGE POSITIVE TO ZERO BEAM THEORY U = 10 M/S ETA = 0·2

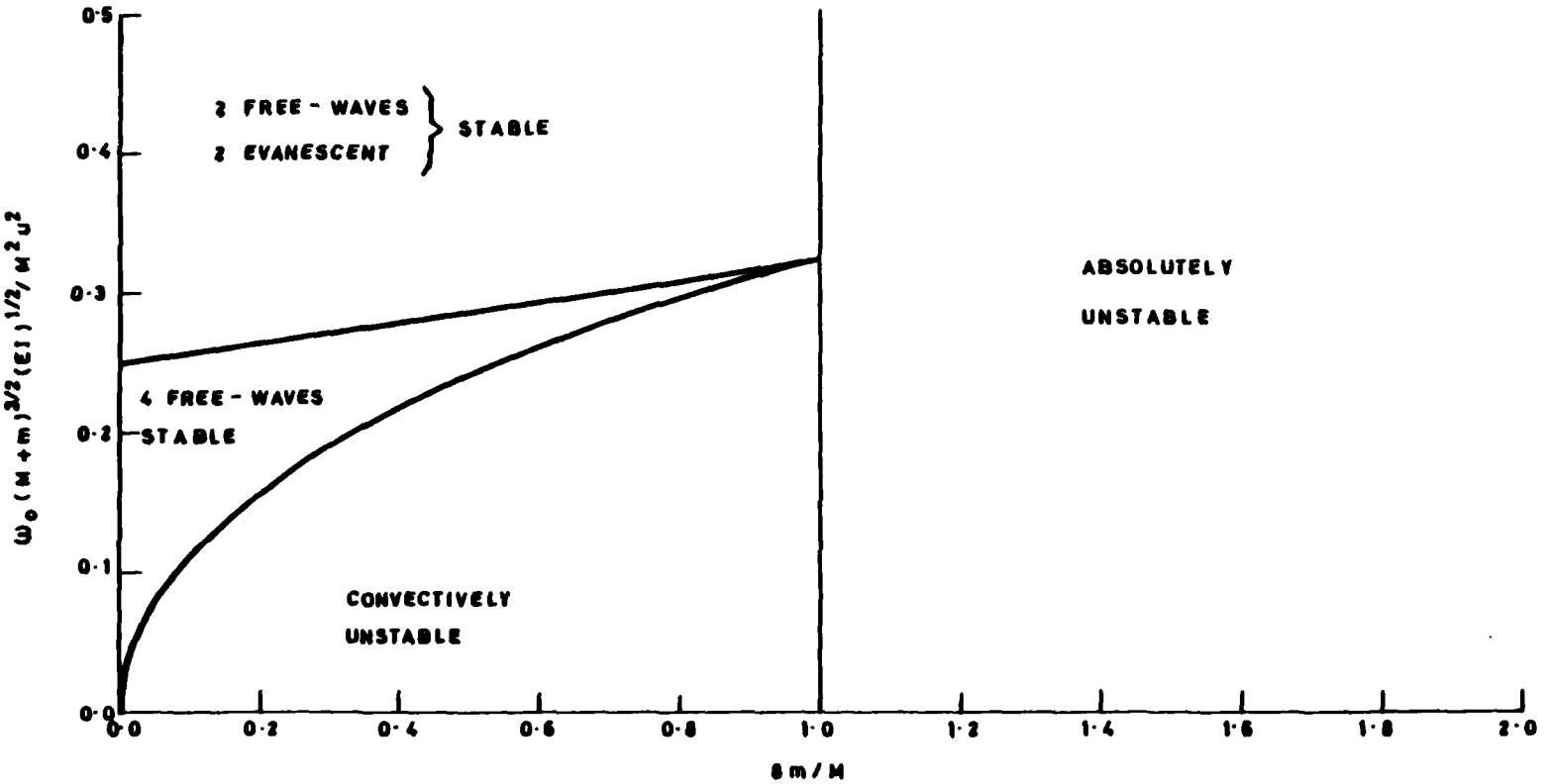

FIG. 12 SUMMARY OF PIPE STABILITY UNDAMPED CASE

A P P E N D I X

A Causal Approach to the Stability Analysis of Linear Systems

In the steady-state approach to stability it is assumed that an excitation of the form $\mathrm{Re}[F_0\exp(-i\omega_0 t)]$ exists for all time t. In practice, however, the excitation will have been switched on at some time, $t=0$, say. Three possibilities for the amplitude of the system response then arise: (i) it may settle down everywhere to finite values which are bounded in both space and time and which may or may not be equal to the steady-state values; (ii) it may settle down everywhere to steady values which increase exponentially with distance from the point of excitation; or (iii) it may grow exponentially with time at every point of the system. Melcher [11] and others have termed case (ii) a convective instability, and case (iii) an absolute instability. The stability analysis proceeds as follows.

It is convenient to represent the system response, $W_r(z,t)$, and the excitation $F_r(z,t)$ as the real parts of complex functions $W(z,t)$ and $F(z,t)$, respectively, viz.,

$$W_r(z,t)=\mathrm{Re}[W(z,t)]$$
$$F_r(z,t)=\mathrm{Re}[F(z,t)] \tag{A1}$$

These functions are then represented as the Laplace-Fourier transform pair

$$\begin{bmatrix} W(z,t) \\ F(z,t) \end{bmatrix} = (1/4\pi^2) \int_{-\omega+i\sigma}^{\omega+i\sigma} \int_{-\infty}^{\infty} \begin{bmatrix} \bar{W}(\alpha,\omega) \\ \bar{F}(\alpha,\omega) \end{bmatrix} \exp(i\alpha z - i\omega t)\, d\alpha\, d\omega \tag{A2}$$

$$\begin{bmatrix} \bar{W}(\alpha,\omega) \\ \bar{F}(\alpha,\omega) \end{bmatrix} = \int_{-\infty}^{\infty} \int_{-\infty}^{\infty} \begin{bmatrix} W(z,t) \\ F(z,t) \end{bmatrix} \exp(-i\alpha z + i\omega t)\, dz\, dt \tag{A3}$$

where σ, a positive constant, is chosen to be such that the line in the complex ω-plane $\mathrm{Im}[\omega]=\sigma$ lies above any singularities of

$$\tilde{W}(z,\omega)=(1/2\pi) \int_{-\infty}^{\infty} \bar{W}(\alpha,\omega)\exp(i\alpha z)\, d\alpha \tag{A4}$$

This ensures that causality is satisfied, i.e. the response of the system is zero for $t<0$.

The Laplace-Fourier transform of the linear differential equation satisfied by the response $W(z,t)$ may be written as

$$D(\alpha,\omega)\bar{W}(\alpha,\omega)=\bar{F}(\alpha,\omega) \tag{A5}$$

where $D(\alpha,\omega)$ is the dispersion relation of the system. Substituting equation (A5) into equation (A2) gives the system response as

$$W(z,t)=(1/4\pi^2)\int_{-\infty+i\sigma}^{\infty+i\sigma}\int_{-\infty}^{\infty}\frac{\bar{F}(\alpha,\omega)}{D(\alpha,\omega)}\exp(i\alpha z-i\omega t)\,d\alpha\,d\omega \tag{A6}$$

The first step in the evaluation of the response $W(z,t)$, is the evaluation of the Fourier (w.r.t. α) integral of equation (A6), which requires information about the behaviour of both $D(\alpha,\omega)$ and $\bar{F}(\alpha,\omega)$. The dispersion relation $D(\alpha,\omega)$ is, in general, a multi-valued function which may be made single-valued on the real α-axis by imposing any radiation condition. In many problems involving fluid-structure interactions, for example, the dispersion relation involves the radical $\sqrt{[(\omega-\alpha U)^2/c^2-\alpha^2]}$ which may be made single valued by imposing the radiation condition that $\mathrm{Im}[\sqrt{[(\omega-\alpha U)^2/c^2-\alpha^2]}]$ should be non-negative on the real α-axis. The (single-valued) dispersion relation on the real α-axis may then be analytically continued into the complex α-plane, where, in order to ensure that the continuation is single-valued everywhere, branch cuts must be introduced. For sufficiently large σ the branch points will be off the real α-axis. The associated branch cuts must not cross the real α-axis and must therefore go to infinity in their respective half-planes. With the exception of this restriction, the choice of branch cuts is arbitrary. The behaviour of $\bar{F}(\alpha,\omega)$ depends only on the type of forcing excitation applied to the system. Two common types of excitation are an impulsive excitation

$$F(z,t)=F_0\delta(z)\delta(t) \tag{A7}$$

whose transform is given by equation (A3) as

$$\bar{F}(\alpha,\omega)=F_0 \tag{A8}$$

and a time-harmonic excitation switched on at $t=0$, viz.,

$$F(z,t)=\begin{cases}0 & t<0\\ F_0\,\delta(z)\exp(-i\omega_0 t) & t>0\end{cases} \tag{A9}$$

whose transform is

$$\bar{F}(\alpha,\omega)=iF_0/(\omega-\omega_0) \tag{A10}$$

The Fourier-integral of equation (A6) may be evaluated by suitably closing the contour and applying Cauchy's theorem. Figure 2 illustrates the case when $z>0$, requiring that the contour is closed in the upper half-plane. For $z<0$ the contour must be closed in the lower half-plane. This convention ensures that, as $\mathrm{Im}[\alpha]$ tends to plus or minus infinity,

respectively, the term $\exp(i\alpha z)$ in the integrand remains finite.

In Figure 2, let α_j^+ $(j=1,N_\alpha)$ represent all the poles of the integrand in the upper half-plane, and α_j^- $(j=1,N_\alpha)$ represent all the poles in the lower half-plane. If σ is sufficiently large then all these poles are well separated from the real α-axis. The contours C_1 and C_2 are circular arcs of large radius and, provided that all these singularities of the integrand in the upper half-plane lie inside the contours, the contributions to the integral from integrating along C_1 and C_2 tend to zero as the radius tends to infinity. The integrals along B_1, B_2, and B_3 are branch cut integrals and will be discussed later. Similar results are true for the contour for $z<0$ in the lower half-plane. The integral may be generally expressed, as the sum of residues and branch cut integrals, in the form

$$\tilde{W}(z,\omega) = \pm i \sum_{j=1}^{N_\alpha} \bar{F}(\alpha_j^\pm,\omega)\exp(i\alpha_j^\pm z)/D'(\alpha_j^\pm,\omega) + \tilde{B}_\alpha(z,\omega) \qquad \text{(A11)}$$

where the + sign corresponds to positive values of z and the - sign to negative values of z. $\tilde{B}_\alpha(z,\omega)$ is the contribution from the integral around the branch cuts in the complex α-plane, and

$$D'(\alpha,\omega)=\partial D(\alpha,\omega)/\partial\alpha$$

The system response $W(z,t)$ is then found by evaluating the Laplace-integral of equation (A6), using the result of the Fourier-integration given by equation (A11). For $t<0$, the contour must be closed as shown in Figure 3a in order to satisfy the causality requirement. For $t>0$, the contour may be closed by using the standard Laplace contour also shown in Figure 3a. Any numerical scheme for evaluating this Laplace integral would become numerically unstable for large positive values of t because of the term, $\exp(\sigma t)$, in the integrand which tends to infinity as t tends to infinity for positive values of σ. It is therefore necessary to deform the contour down to the real ω-axis by letting σ tend to zero, not only to allow a numerical evaluation of the integral, but also in order to identify the contributions to the integral from branch cuts and poles in the complex ω-plane. The resulting contour, shown in Figure 3b, lies just below the real ω-axis, but is indented around any poles and branch points in the upper half-plane or on the real ω-axis. If ω_n $(n=0,N_\omega)$ represent all the poles of the integrand, then the system response, for $t>0$, may be expressed using Cauchy's theorem, as the sum of residues and branch cut integrals, in the form

$$W(z,t) = \sum_{n=0}^{N_\omega}\{-i\hat{B}_\alpha(z,\omega_n)\pm\sum_{j=1}^{N_\alpha} R(\alpha_j^\pm,\omega_n)\exp(i\alpha_j^\pm z)\}\exp(-i\omega_n t) + B_\omega(z,t) \qquad \text{(A12)}$$

where $R(\alpha_j^\pm,\omega_n)$ and $\hat{B}_\alpha(z,\omega_n)$ are the residue contributions, defined as

$$R(\alpha_j^\pm,\omega_n) = \lim_{\omega\to\omega_n}\{(\omega-\omega_n)\bar{F}(\alpha_j^\pm,\omega)/D'(\alpha_j^\pm,\omega)\} \qquad \text{(A13)}$$

$$\hat{B}_\alpha(z,\omega_n)=\lim_{\omega\to\omega_n}\{(\omega-\omega_n)\tilde{B}_\alpha(z,\omega)\} \qquad (A14)$$

and $B_\omega(z,t)$ is the contribution from the integral around the branch cuts in the complex ω-plane.

In order to deform the contour in the ω-plane as described above, the continuation of $\tilde{W}(z,\omega)$ into the region $Im[\omega]<\sigma$ must be analytic. As the Laplace contour is moved down to the real ω-axis, the poles enclosed by the Fourier contours also move in the α-plane and it may be necessary to deform the Fourier contours so that they always include the same poles of the response transform, $\bar{W}(\alpha,\omega)$.

In order to ascertain whether or not any physical significance can be attached to each term of equation (A12) for the response of the system, it is necessary to use the root locus technique as described by Melcher [11] and Atkins [14]. Firstly, consider the contribution from a simple pole on the real ω-axis at $\omega=\omega_n$, which arises from a time-harmonic excitation of the form $F_0\exp(-i\omega_n t)$. In the root locus technique the loci of roots $\alpha_j^{\pm}$ (which are functions of ω) are plotted for values of $\omega=\omega_r+i\sigma$ for particular values of ω_r as σ varies from $+\infty$ to 0. Provided that these loci do not coalesce (i.e. intersect at the same value of ω_r and σ) for any real ω_r then there are twelve basic possibilities for each locus which are illustrated in Figure 4a. The shaded circles in this Figure denote points where the loci terminate, corresponding to $\sigma=0$.

The form of the system response may be determined from the loci for which $\omega_r=Re[\omega_n]$. In cases (1) to (6), because each of the loci comes from above the real α-axis the Fourier contour must be indented where necessary to include the pole in the upper contour. The response due to each of these poles is non-zero only for $z>0$, in which case it is given by

$$W(z,t)=F_0\exp\{(i\alpha_r-\alpha_i)z\}\exp(-i\omega_n t) \qquad (A15)$$

where $\alpha_r+i\alpha_i$ is the location of the pole when $\sigma=Im[\omega_n]=0$.

In cases (1)-(3), where $\alpha_r>0$, the phase disturbance propagates in the positive z-direction. If $\alpha_i>0$, as in case (1), the wave decays exponentially with distance and it is called an evanescent wave. If $\alpha_i=0$, as in case (2), the wave propagates without decay. In case (3), where $\alpha_i<0$, the wave increases exponentially with z and is termed 'convectively unstable'. In cases (4)-(6),where $\alpha_r<0$, the phase disturbance propagates in the negative z-direction (i.e. towards the excitation). In case (4), where $\alpha_i>0$, as the phase propagates the wave amplitude increases exponentially with distance. In case (5) $\alpha_i=0$ and the wave propagates without decay. If $\alpha_i<0$, as in case (6), the wave decays exponentially with distance.

Cases (7)-(12) are similar to cases (1)-(6), except that the loci come from below the real α-axis and the Fourier contours must be indented where necessary to ensure that, in each case, these poles are included in the lower contour. The contribution to the response from each of these poles is therefore non-zero only for $z<0$.

The contributions to the displacement from simple poles in the complex ω-plane represent propagating, spatially amplifying or spatially decaying waves at the excitation frequency, ω_n. This description of the propagation directions gives only the phase speeds of the individual waves. A more realistic quantity physically is the group velocity, $\partial\omega/\partial\alpha$, the velocity at which energy propagates. This may be obtained from the direction of the loci at $\sigma=0$, viz.,

$$\partial\omega/\partial\alpha=\partial(i\sigma)/\partial(\alpha_r+i\alpha_i)=[(\partial\alpha_i/\partial s)+i(\partial\alpha_r/\partial s)](\partial\sigma/\partial s) \qquad (A16)$$

where s is the arc length along the locus, measured from $\sigma=0$. In particular, the group velocity is positive if the initial direction of the locus in the complex α-plane is upward, and the group velocity is negative if the initial direction of the locus is downward.

In order to consider the contribution, $B_\omega(z,t)$, to the response from the integrals around the branch cuts in the complex ω-plane possible singularities in the complex ω-plane must be identified. Equation (A11) indicates that singularities in the ω-plane may be expected if, for some ω

$$D'(\alpha_j(\omega),\omega)=0 \qquad (A17)$$

where $\alpha_j(\omega)$ is a root of the dispersion relation

$$D(\alpha_j(\omega),\omega)=0 \qquad (A18)$$

If a solution to the simultaneous equations (A17) and (A18) exists, with $\mathrm{Im}[\omega]>0$, it indicates that equation (A18) has a repeated root α_j at that value of ω, which in the context of the root-locus method means that two root loci coalesce in the complex α-plane. There are two distinct possibilities here as illustrated in Figure 4b. If both loci have come from either above or below the real α-axis, as in case (1), then the Fourier contour in the complex α-plane may always be deformed to include both poles, and at the coalescence frequency the residue may be calculated as for a second order pole at $\alpha=\alpha_j(\omega)$: this constitutes a removable singularity in the complex ω-plane. Thus, as pointed out by Melcher [11], the coalescence of poles illustrated in case (1) does not indicate a true singularity in the complex ω-plane. In case (2), however, a locus originating above the real α-axis coalesces with one originating from below. The Fourier contours in the complex α-plane can no longer be distorted to include only the poles originating in the upper (or lower) half-plane, and they become 'pinched' at the (complex) frequency, ω_p, at which coalescence occurs. This confirms the presence of a singularity in the complex ω-plane at $\omega=\omega_p$, which may be identified as a branch point by considering the Taylor series expansion of the dispersion relation about $\omega=\omega_p$, $\alpha=\alpha_p$, viz.,

$$D(\alpha,\omega)=(\omega-\omega_p)\partial D/\partial\omega+(1/2)(\alpha-\alpha_p)^2\partial^2 D/\partial\alpha^2+(\alpha-\alpha_p)(\omega-\omega_p)\partial^2 D/\partial\alpha\partial\omega$$

$$+(1/2)(\omega-\omega_p)^2\partial^2 D/\partial\omega^2+\cdots\cdots \qquad (A19)$$

where all the derivatives are to be evaluated at $\alpha=\alpha_p$, $\omega=\omega_p$. By considering the order of each of the terms in equation (A19) as $\omega\to\omega_p$, Melcher [11] has shown that in a neighbourhood of (α_p,ω_p)

$$(\alpha-\alpha_p)=\pm[2(\omega-\omega_p)(\partial D/\partial\omega)/(\partial^2 D/\partial\alpha^2)]^{1/2} \qquad (A20)$$

The residue contribution to $\tilde{W}(z,\omega)$ in the neighbourhood of (α_p,ω_p), is given by equation (A11) as

$$\pm i\bar{F}(\alpha,\omega)\exp(i\alpha z)/D'(\alpha,\omega) \qquad (A21)$$

Differentiation of the Taylor expansion, equation (A19), with respect to α allows the residue contribution, equation (A21), to be written to first order in $(\alpha-\alpha_p)$ as

$$\pm i\bar{F}(\alpha,\omega)\exp(i\alpha z)/((\alpha-\alpha_p)\partial^2 D/\partial\alpha^2) \qquad (A22)$$

which may be expressed in terms of ω, using equation (A20), as

$$\pm i\bar{F}(\alpha,\omega)\exp(i\alpha z)/[2(\omega-\omega_p)(\partial^2 D/\partial\alpha^2)(\partial D/\partial\omega)]^{1/2} \qquad (A23)$$

demonstrating that ω_p is, in fact, a branch point of $\tilde{W}(z,\omega)$.

In the context of the root-locus method, the presence of the branch cut may be demonstrated by considering the possible behaviour of neighbouring root-loci in the complex α-plane for ω_- and ω_+, where $\omega_-<\mathrm{Re}[\omega_p]$ and $\omega_+>\mathrm{Re}[\omega_p]$, as illustrated in Figure 5a and 5b. In both cases, it may be shown that the residue contributions to the Fourier integral $\tilde{W}(z,\omega)$ are discontinuous at $\mathrm{Re}[\omega]=\mathrm{Re}[\omega_p]$, indicating that the branch cut in the complex ω-plane runs from ω_p to $\omega_p-i\infty$. This choice of branch cut is imposed by the causality requirement which determines the poles to be included in each Fourier contour.

The approximate value of the contribution to the response from the integration around the branch cut in the complex ω-plane may be calculated by making the assumption that $\bar{F}(\alpha,\omega)$ may be approximated by $\bar{F}(\alpha_p,\omega_p)$. This approximation is exact for an impulsive excitation, and the branch cut integral then becomes

$$B_\omega(z,t) = \frac{\pm i\bar{F}(\alpha_p,\omega_p)\exp(i\alpha_p z)}{\pi[2(\partial^2 D/\partial\alpha^2)(\partial D/\partial\omega)]^{1/2}} \int_{\omega_p-i\infty}^{\omega_p} \frac{\exp(-i\omega t)}{(\omega-\omega_p)^{1/2}}\,d\omega \qquad (A24)$$

which can be evaluated analytically as

$$B_\omega(z,t) = \frac{\pm i(1-i)\bar{F}(\alpha_p,\omega_p)\exp(i\alpha_p z-i\omega_p t)}{2[\pi(\partial^2 D/\partial\alpha^2)(\partial D/\partial\omega)]^{1/2}t^{1/2}} \qquad (A25)$$

Equation (A25) shows that if the imaginary part of ω_p is positive

the contribution to the response from the branch cut integral grows exponentially with time at all locations, z. This is termed an absolute instability, and occurs whatever the value of the excitation frequency, ω_n, and in fact it also occurs for an impulsive excitation. When a system is absolutely unstable, the system response is always dominated by the 'pinch' frequency and wavenumber, ω_p and α_p respectively, after a sufficiently long time interval. If ω_p is real then the factor $t^{-1/2}$ in equation (A25) ensures that the response is transient.

It is now necessary to discuss the branch cut integrals in the complex α-plane. In general, provided that the branch cuts are well away from any singularities of the integrand, the integral around the circular contour B is zero, and the integrals along the contours B_1 and B_3 contribute only to the near fields because the integrands are bounded. Crighton [3] has pointed out that only those poles which exist for all suitable choices of the branch cuts may have any physical significance at large values of z. The remaining poles contribute only to the near field and their contributions must always be combined with those from the branch cut integrals. The precise form of the branch cut integrals depends on the choice of branch cuts and on the form of the dispersion relation.

As already mentioned, if σ is sufficiently large all the poles of the integrand of equation (A6) are well separated from the real α-axis. A consequence of this is that the location of the poles depends on a particular choice of branch cuts, and that no pole exists for all possible choices of branch cuts. It also means that, as σ varies, a root locus corresponding to the movement of a particular pole may cross a branch cut and 'disappear', or vice-versa. At $\sigma=0$, the poles corresponding to evanescent waves also depend on the choice of branch cuts. The contribution to the response from these poles can therefore have no physical significance in isolation, but must be combined with the branch cut integrals. A free-wave pole (i.e. one which lies on the real α-axis for $\sigma=0$) always exists for all possible choices of branch cut and therefore has physical significance. A pole corresponding to a convective instability crosses the real α-axis at some positive value of σ and therefore always exists in a neighbourhood of the axis. Furthermore, according to Atkins [14], if coalescing poles in the α-plane corresponding to a singularity in the upper-half ω-plane exist, they do so for all possible choices of branch cut.

In the absence of branch cuts in the complex α-plane, however, the location of all the complex poles in the α-plane may be uniquely determined, and their contributions to the response may be identified as propagating, evanescent or convectively amplifying waves.

To summarize, the root locus technique may be used to determine the stability characteristics of a linear system. Firstly, it is necessary to plot the root loci for a range of frequencies in order to determine whether or not there is a branch point in the complex ω-plane as a result of coalescing poles whose loci in the α-plane come from opposite half-planes. If such a branch point exists the system is absolutely unstable and the response, which is predominantly at the branch point frequency ω_p grows exponentially with time at all locations. If no such branch point exists, the response of the system may be determined by the root loci in the α-plane

which correspond to the excitation frequencies. The modes of the response may be identified as non-decaying travelling waves or convectively amplifying waves, and, in cases where there are no branch points in the α-plane, evanescent waves may also be identified. In practice instabilities are usually damped by some non-linear mechanism, or other factors not taken into account in the current theory.

A necessary, but not sufficient, condition for instability (absolute or convective) is that a locus in the α-plane crosses the real α-axis. This implies that for some real wavenumber α, the dispersion relation must have a root ω with a positive imaginary part. This is the criterion which is usually used to determine instability using the steady-state approach.

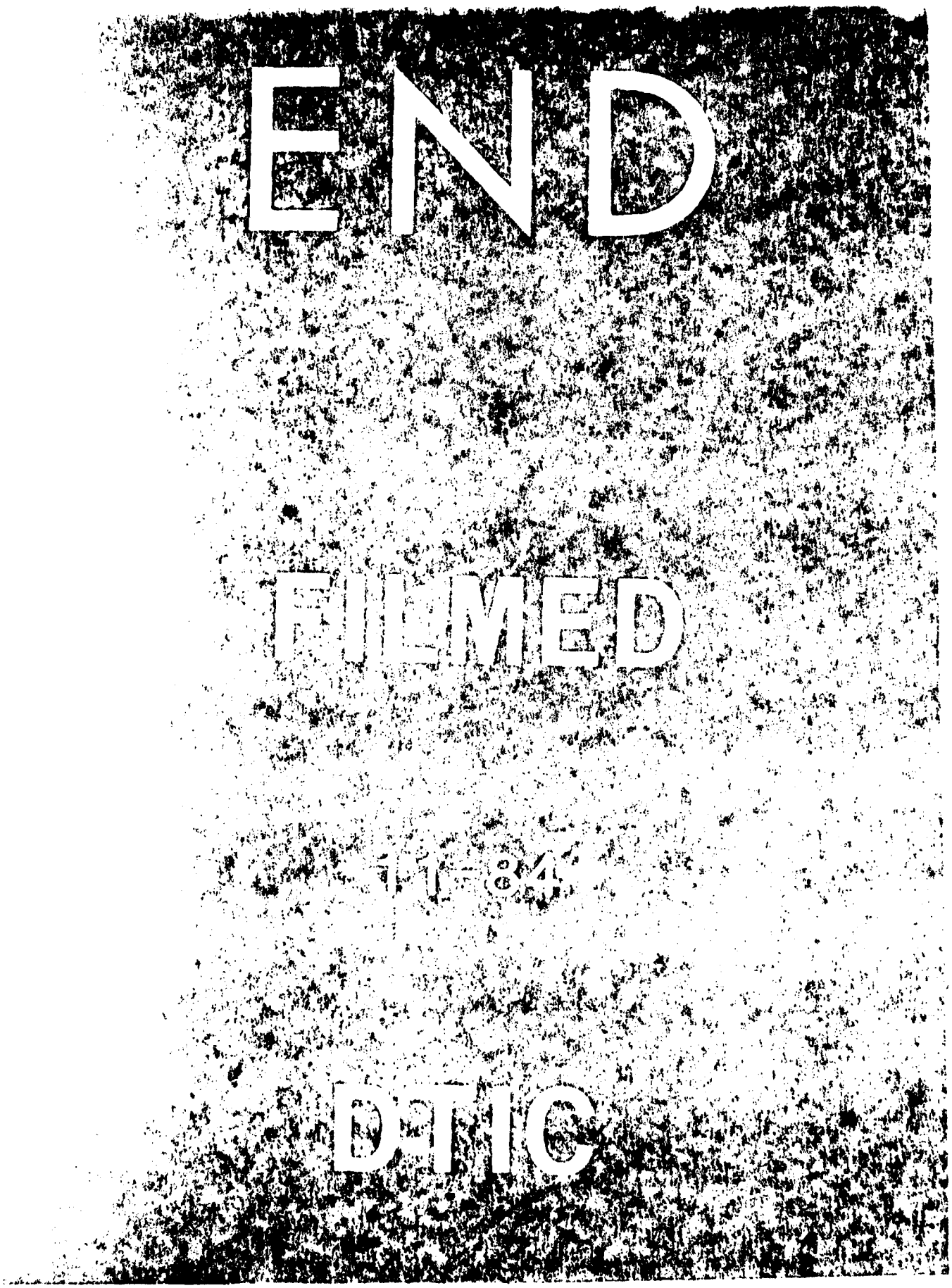
END
FILMED
DTIC